JOURNAL OF MATERIALS SCIENCE 28 (1993) 4562–4570

A crystal phase study of zinc hydroxide chloride in electric-arc-furnace dust

CHUNG-LEE LI, MIN-SHING TSAI
Institute of Minerals, Metallurgy and Materials Science, National Cheng-Kung University, Tainan, Taiwan

Chemical analysis shows that electric-arc-furnace (EAF) dust obtained from 13 steelmaking factories in Taiwan is composed chiefly of Fe (15–37%), Zn (7–28%) and Mn (1.55–3.99%) and that the mineral composition is mainly (Mn, Zn) Fe_2O_4, ZnO and $ZnCl_2 \cdot 4Zn(OH)_2 \cdot H_2O$. It was also found that EAF dust exists as irregular agglomerates from 3 to 20 μm in size and are made up of much smaller round particles from 0.3 to 1 μm in size. $ZnCl_2$ gas in the dust condenses after passing through the EAF gas-cooler system binding small particles of Mn–Zn ferrite together. The agglutinative substance was identified as being $ZnCl_2 \cdot 4Zn(OH)_2 \cdot H_2O$ possibly arising from the interaction between $ZnCl_2$ and ZnO adhering to the Mn–Zn ferrite particles; a conjecture supported by the fact that EAF dust dissolves easily in hydrochloric-acid solution leaving only loosely aggregated Mn–Zn ferrite material.

1. Introduction

In the electric arc furnaces (EAFs) approximately 1–2% of each charge is converted to dust. The USA produces an estimated 500 000–510 000 tons and Taiwan produces 60 000 tons of dust per year [1, 2]. Recycling and disposal of dust is complicated not only because it contains large amounts of such heavy metals as lead, cadmium and chromium, but also because it is extremely fine and difficult to handle.

In a study characterizing 32 bulk samples of EAF dust from the USA [1], only three of the samples were under the limits set by EPA, the others failing the test for Cd, Cr and Pb. In fact, all EAF dust is now classified as hazardous waste material under USA Environmental Protection Administration (EPA) regulations. Not surprisingly then, the treatment or disposal of EAF dust has been the focus of increased attention in recent years, during which many methods have been proposed to recover zinc (a major component), including pyrometallurgical [2, 3–5] and hydrometallurgical processes [6–10].

Studies on the crystalline and microstructural properties of EAF dust are sparse, hindering the development of more economical recovery processes. This study used X-ray diffraction (XRD), scanning electron microscopy (SEM), infrared (i.r.) spectroscopy and auger electron spectroscopy (AES) to acquire crystalline and microstructural information pertinent to improving the treatment processes used to recover various materials from EAF dust.

2. Experimental procedure

2.1. Sample and analytical methods

EAF dust samples used in these experiments were obtained from dust containers located at the bottom of baghouses in a number of Taiwanese steelmaking plants.

The cationic composition of EAF dust was determined by an atomic absorption (AA) spectrometric analyser (Perkin-Elmer 3030). Anions were determined after Na_2CO_3 fusion, which converted water-insoluble anions such as SO_4^{2-} and NO_3^- to the water-soluble sodium form and converted the transition metals to their corresponding carbonate species which are generally insoluble in water [1]. This chemical conversion generates anionic compounds which can be rapidly identified by high-performance liquid chromatography (HPLC).

The crystalline phase was determined by XRD using FeK_α radiation (RIGAKU D/MAX IIB). Loose particle samples were prepared for microscopy and chemical-composition evaluation by first dispersing $10–20 \times 10^{-6}$ kg of EAF dust in a few millilitres of distilled water. While sonicating, a sample of the dispersion was withdrawn with a pipette and one drop was placed on a polished carbon plate, allowed to dry, and then coated with either carbon or gold. SEM and electron probe X-ray microanalysis EPMA of these particles were performed using models JSM-840 and JSM-35/LINKS AN 10000/85. A method in which whole particles were dispersed between two carbon films on a standard copper specimen grid was used to prepare EAF dust for scanning transmission electron microscopy (STEM, Hitachi H700-H). AES was used to analyse surface composition. I.r. spectra of the compounds were obtained by using the standard KBr disc technique in a Hitachi 270-30 i.r. spectrophotometer.

2.2. Leaching test

Distilled water and reagent-grade HCl were used to prepare the leaching solution. Leaching of CS1 (carbon-steel test number one, see later) dust was carried

0022–2461

out over different HCl concentrations using a solid/liquid mass ratio of 1/10, 2 h leaching time and a stirring speed of 200 r.p.m. Fe, Zn and Mn concentrations in the solution were measured with the atomic absorption spectrometer mentioned above.

3. Results and discussion

3.1. Characterization of EAF

3.1.1. Chemical analysis

Chemical quality analysis by emission spectrometer showed that EAF dust in Taiwan is composed chiefly of Fe, Zn and Mn, and to a lesser extent Pb, Cd, Cu, Ni, Cr, Ca, K, Si, Cl and S. Those elements which appeared in emission spectrometer analysis were further analyzed by AA. The complete chemical analysis is presented in Table I. EAF dust from 13 steelmaking factories is divided into two categories depending on whether it came from carbon-and-low alloy steel (CS), or stainless steel (SS). CS dust consisted mainly of Fe (19–30%), Zn (20–28%), Pb (1.2–3.2%) and Mn (1.6–4.0%), whereas SS consisted mainly of Fe (15–37%), Zn (1.6–12.8%), Pb (0.68–1.70%) and Mn (1.8–7.7%). CS dust tends to be richer in Zn and Pb because of the principal use of post-consumer scrap as well as galvanized and other coated products in the melt, whereas SS dust contained greater amounts of Mn, Ni and Cr since scrap alloy is the principal metal in the melt. Eacott *et al.* [6] reported that in the USA CS dust is composed of 25–47% Fe, 11–27% Zn, 1.0–3.8% Pb, 2.5–4.6% Mn and less than 1% of Cr, Cu, Ni and Cd, whereas, SS dust is composed of 22–36% Fe, 1.8–6.2% Zn, 2.4–4.6% Mn and less than 1% each of Cr, Cu and Ni. In addition, less than 10% each of Ca, Mg, Si, K, Na, Cl^- and SO_4^{2-} were also found in both CS and SS dust. Stephen *et al.* [1] examined the dust from 32 USA EAFs, and found that the content of Cl^- and SO_4^{2-} was between 1.0 and 5.0% and 1.0 and 2.5%, respectively. The above results indicate that both Taiwan and USA EAF dust are similar in chemical composition.

3.1.2. Specific-gravity and sieve analysis

Specific-gravity analysis of the EAF dust generated values between 3.43 and 4.34, with the average being about 4.00. Sieve analyses showed that more than 94% of the dust is finer than 325 mesh size. Using the Brunquet–Emett–Teller method (BET), the specific surface area was determined to be around 1–2 $\times 10^3\,kg^{-1}$, which is equivalent to an average particle diameter of about 1–2 μm. The specific gravity and specific surface area of 32 USA EAF dusts, also examined by Stephen *et al.* [1], were found to be around 3.25–4.82 (with an average of 4.4) and 2–4 $\times 10^3\,m^2\,kg^{-1}$, respectively. Thus, it is feasible to compare the specific gravity and specific surface area of Taiwanese EAF dust with their USA counterparts.

3.1.3. Morphology of EAF dust

Figs 1 and 2 are SEM micrographs of CS1 and CS4 dust, respectively. As can be seen, EAF dust ranges in size from 3–20 μm, being irregular agglomerates of much smaller particles (0.3–1 μm in size). (The TEM CS1 dust micrograph (Fig. 10) clearly shows that the spherical particles are bound together. The other samples, as well as samples of dust from the USA [1], all demonstrated similar behaviour.)

3.1.4. Crystal phases

The XRD patterns of a number of EAF dusts are shown in Fig. 3. Note that the major phases are ZnO and spinel ferrite, whose peaks are very close to those of Fe_3O_4, $ZnFe_2O_4$ and (Mn, Zn) Fe_2O_4. These results are supported by numerous investigators [1, 3, 6, 7, 9, 11].

Following a suggestion of Thomas and Fray [9], namely that the spherical particles of EAF dust were composed of $ZnFe_2O_4$, the spherical particles in CS9 and SS1 dust were analysed using SEM and EPMA, and the SEM results are presented in Figs. 4 and 5 and the EMPA results in Tables II and III for CS9 and SS1 dust, respectively. In addition, the small spherical particles forming the irregular agglomerates of CS1 dust were also analysed (using SEM and line scanning), and the results presented in Fig. 6. An examination of the results revealed that while ZnO, MnO, FeO and Fe_2O_3 constitute the major components of the spherical particles, they are not consistently specified in the ferrite particles. It is therefore reasonable to

TABLE I Content of elements in EAF dust

	Fe (%)	Zn (%)	Mn (%)	Pb (%)	Cr (%)	Cu (%)	Ca (%)	Si (%)	Mg (%)	Na (%)	K (%)	Cl^- (%)	SO_4^{2-} (%)	Ni (p.p.m.)	Cd (p.p.m.)
CS1	30.32	20.73	3.74	1.90	0.30	0.22	1.93	1.71	1.36	1.95	1.25	3.95	2.34	221	538
CS2	19.93	22.50	1.55	2.56	0.23	0.24	2.52	1.17	0.56	1.51	1.32	4.86	2.10	306	357
CS3	18.95	24.65	3.84	2.16	0.38	0.35	2.27	1.38	0.67	2.28	1.27	2.32	2.11	428	9600
CS4	19.04	20.17	3.99	1.15	0.24	0.20	4.70	2.09	2.78	1.20	1.28	2.98	3.25	308	338
CS5	22.38	27.32	2.77	2.93	0.62	0.28	2.27	1.32	0.44	2.08	1.68	7.00	1.30	294	326
CS6	23.56	27.79	3.28	3.20	0.47	0.22	2.32	1.31	1.01	1.82	1.46	7.14	2.40	350	429
CS7	22.70	26.85	2.49	2.12	0.18	0.32	0.94	1.23	0.80	1.95	1.40	–	–	310	2200
CS8	28.78	20.16	2.76	1.61	0.19	0.32	2.50	1.83	2.27	5.63	1.00	–	–	317	1900
CS9	18.70	24.60	2.04	1.70	0.22	0.20	4.29	1.42	2.58	2.46	1.61	2.95	1.78	226	1100
SS1	37.11	12.08	3.18	0.68	0.28	0.26	4.97	1.36	1.60	1.01	0.47	5.20	2.47	552	979
SS2	35.56	12.76	1.81	1.11	0.57	0.22	4.52	2.76	0.83	0.77	0.46	2.19	2.27	487	137
SS3	15.02	7.31	7.65	0.72	0.34	0.23	7.99	1.27	8.47	1.21	0.79	3.35	2.12	3100	195
SS4	27.20	6.83	6.40	1.66	0.41	0.11	3.07	4.51	6.33	1.24	2.52	–	–	450	183

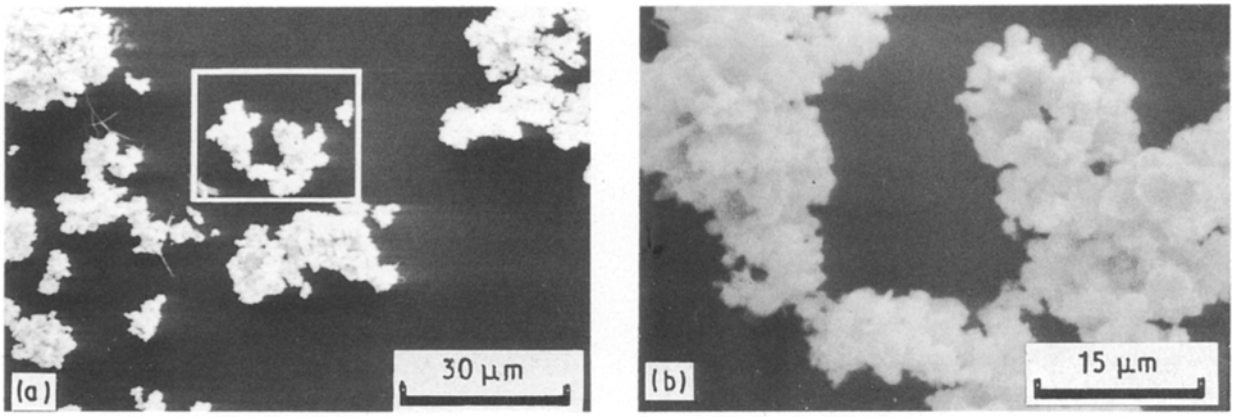

Figure 1 SEM micrographs of CS1 dust.

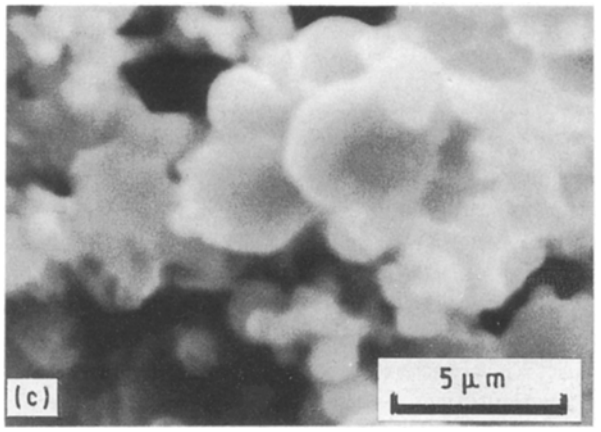

TABLE II EPMA analysis of CS9 dust (manganese oxide is $(Mn_{0.31}Zn_{0.09}Fe_{0.60})Fe_2O_4$

Iron oxide	81.8%
Zinc oxide	3.3%
Manganese oxide	11.7%

TABLE III EPMA analysis of SS1 dust (manganese oxide is $(Mn_{0.05}Zn_{0.19}Fe_{0.76})Fe_2O_4$

Iron oxide	90.7%
Zinc oxide	7.7%
Manganese oxide	1.7%

assume that the small spherical particles are composed of various components of (Mn, Zn, Fe) Fe_2O_4 ranging in size from 1 to 30 μm.

In addition to Mn–Zn ferrite and ZnO, the compound $ZnCl_2 \cdot 4Zn(OH)_2$ may also exist, as evidenced by the presence of several weak peaks in the XRD pattern of EAF dust (see Fig. 3). However, since previously reported results [1, 3, 6, 7, 9, 11] make no mention of this component, differential thermal analysis (DTA) or thermogravimetric analysis (TGA), i.r. and AES analyses were carried out in order to confirm the XRD results.

DTA/TGA results of CS1 dust are presented in curve (b) Fig. 7, which shows endothermic peaks at 127, 210 and 262 °C. Note that weight loss occurred at these temperatures, but became insignificant when the temperature exceeded 262 °C. The results of DTA/TGA reported by Srivastava and Secco [12], for $ZnCl_2 \cdot 4Zn(OH)_2 \cdot H_2O$ and $ZnCl_2 \cdot 4Zn(OH)_2$ are shown in curve (b) of Fig. 7. The endothermic peak at 127 °C denotes the dehydration of $ZnCl_2 \cdot 4Zn(OH)_2 \cdot H_2O$ which proceeds in two steps that result in peak temperatures of 187 °C and 200 °C. The second endothermic centre (at 262 °C) results from the melting of $ZnCl_2$, while the final one is due to the vaporization of liquid $ZnCl_2$ at a peak temperature of 708 °C.

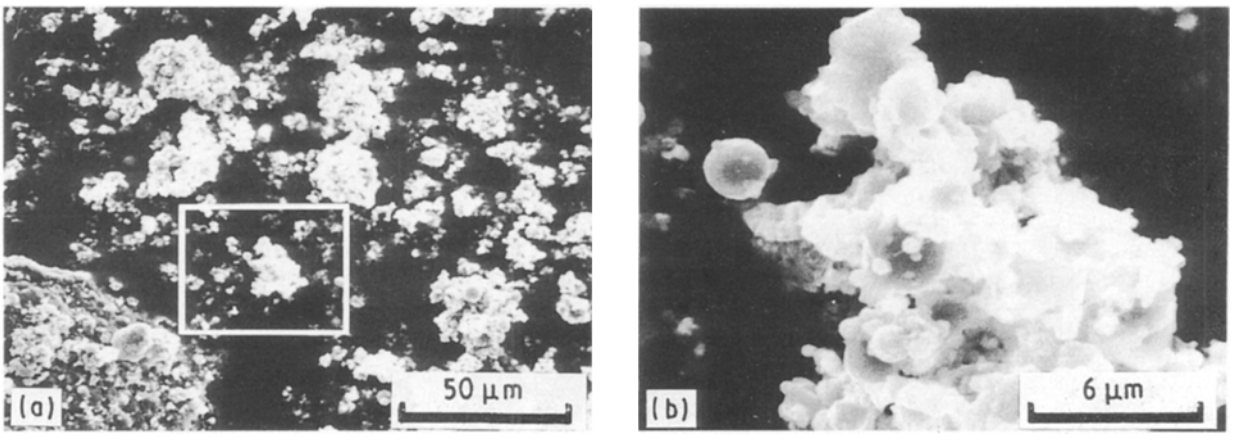

Figure 2 SEM micrographs of CS4 dust.

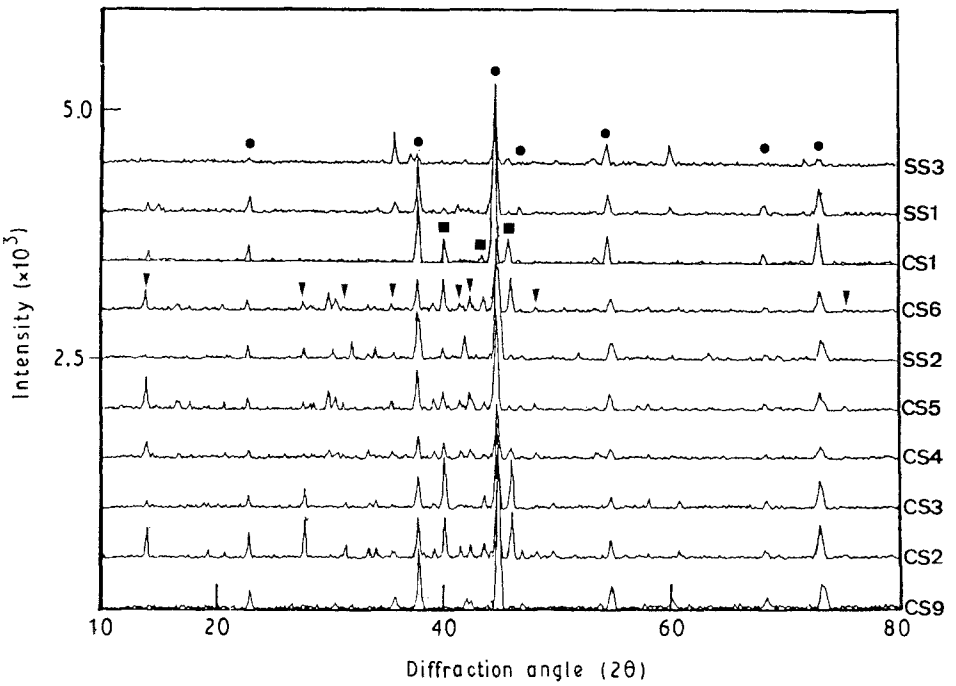

Figure 3 XRD patterns of EAF dust: (●) spinel ferrite, (■) ZnO, (▼) $ZnCl_2 \cdot 4Zn(OH)_2$.

$$ZnCl_2 \cdot 4Zn(OH)_2 \cdot H_2O \xrightarrow{110-147\,^\circ C} ZnCl_2 \cdot 4Zn(OH)_2 + H_2O \ldots \quad (1)$$

$$ZnCl_2 \cdot 4Zn(OH)_2 \xrightarrow{167-266\,^\circ C} 4ZnO + ZnCl_2 + 4H_2O \ldots \quad (2)$$

A comparison of curves (a), (b) of Fig. 7, reveals that the CS1 dust peak temperatures of 127, 187, 210 and 262 °C are in complete agreement with those expected of $ZnCl_2 \cdot 4Zn(OH)_2 \cdot H_2O$. Note that the absence of a 708 °C peak may not mean the absence of zinc hydroxide chloride in CS1 dust, as it may be present in such a small amount as to be undetectable. In fact, in accordance with the DTA/TGA, the XRD pattern of EAF dust calcined at 600 °C for 4 h (see Fig. 8), clearly shows that the diffraction peaks of $ZnCl_2 \cdot 4Zn(OH)_2$ have disappeared.

The strong peaks of spinel ferrite and ZnO and the weaker peaks of $ZnCl_2 \cdot 4Zn(OH)_2$ exist in the XRD patterns of EAF dust. In order to conclusively identify the presence of $ZnCl_2 \cdot 4Zn(OH)_2$, its i.r. spectrum was run, since it is well known that O–H stretching gives rise to a strong absorption band in the 3700–3500 cm^{-1} region, while oxides are usually non-absorbing above 1000 cm^{-1}. I.r. spectra of EAF dust are presented in Fig. 9, where spinel ferrite is denoted by bands localized at 585 and 465 cm^{-1} (close to Fe_3O_4 and $ZnFe_2O_4$ [13, 14, 15]). The absorption bands of ZnO occur at 615, 535 and 440 cm^{-1} [14], but are not very distinct, being either just resolved or very broadened, and hence difficult to identify. I.r. spectra obtained by Srivastava and Secco [16] demonstrate strong bands at 3600, 3590, 3540, 3480, 870 815, 695 and 580 cm^{-1} for $ZnCl_2 \cdot 4Zn(OH)_2$ (curve B of Fig. 9), and at 3520, 3480, 895, 715 and 560 cm^{-1} for $ZnCl_2 \cdot 4Zn(OH)_2 \cdot H_2O$ (curve A of Fig. 9). Note that the spectra of $ZnCl_2 \cdot 4Zn(OH)_2$ and $ZnCl_2 \cdot 4Zn(OH)_2 \cdot H_2O$ exhibit similar features except that the major band between 3600 and 3400 cm^{-1}, which can be seen as a faintly discernible doublet in the hydrate, is resolved upon dehydration into a prominent doublet [16]. Thus, our i.r. spectra (also presented in Fig. 9), indicate that at least a trace of $ZnCl_2 \cdot Zn(OH)_2$ or $ZnCl_2 \cdot 4Zn(OH)_2 \cdot H_2O$ exists in EAF dust.

The "free"-hydroxyl stretching vibration is distinguishable from the O–H stretching vibration in water by the reduced frequency and increased broadening of the latter. In the case of water hydration (crystallization), there is less chance of hydrogen-bonding effects, and thus vibrational stretching and bending are observed in the region 3600–3200 cm^{-1} and near 1650 cm^{-1}, respectively. Conversely, in the case of absorbed water, the vibrational stretching and bending appear, respectively, as a single broad absorption band in the 3400–3200 cm^{-1} region, and as a weak absorption in the 1650–1600 cm^{-1} region [13]. I.r. results confirmed the presence of $ZnCl_2 \cdot 4Zn(OH)_2 \cdot H_2O$ due to the broad absorption in the 3700–3300 cm^{-1} region, and the strong band at 1650 cm^{-1}. In addition, DTA/TGA further substantiated these results.

Stephen *et al.* [1] suggested that surface charge and magnetic properties caused the agglomeration of EAF dust particles. EAF dust examined by TEM (see Fig. 10), clearly shows two particles agglomerated by some sort of binding substance. Because this substance is too thin for SEM chemical qualitative analysis, AES was used and the results presented in Fig. 11. Note the presence of elements Si, Cl, C, Ca, O, Mn, Fe and Zn. SIMS chemical analysis also indicated that the CS1 dust particle surface contains H, O, Na, Ca, SiO_2,

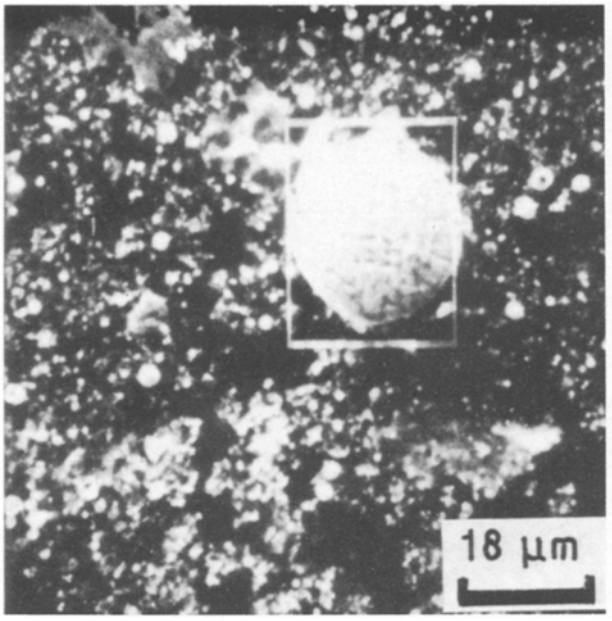

Figure 4 SEM micrograph of CS9 dust.

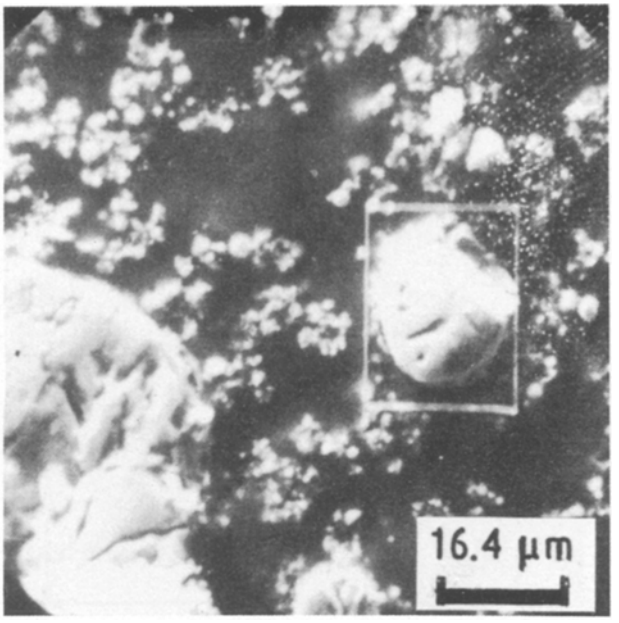

Figure 5 SEM micrograph of SS1 dust.

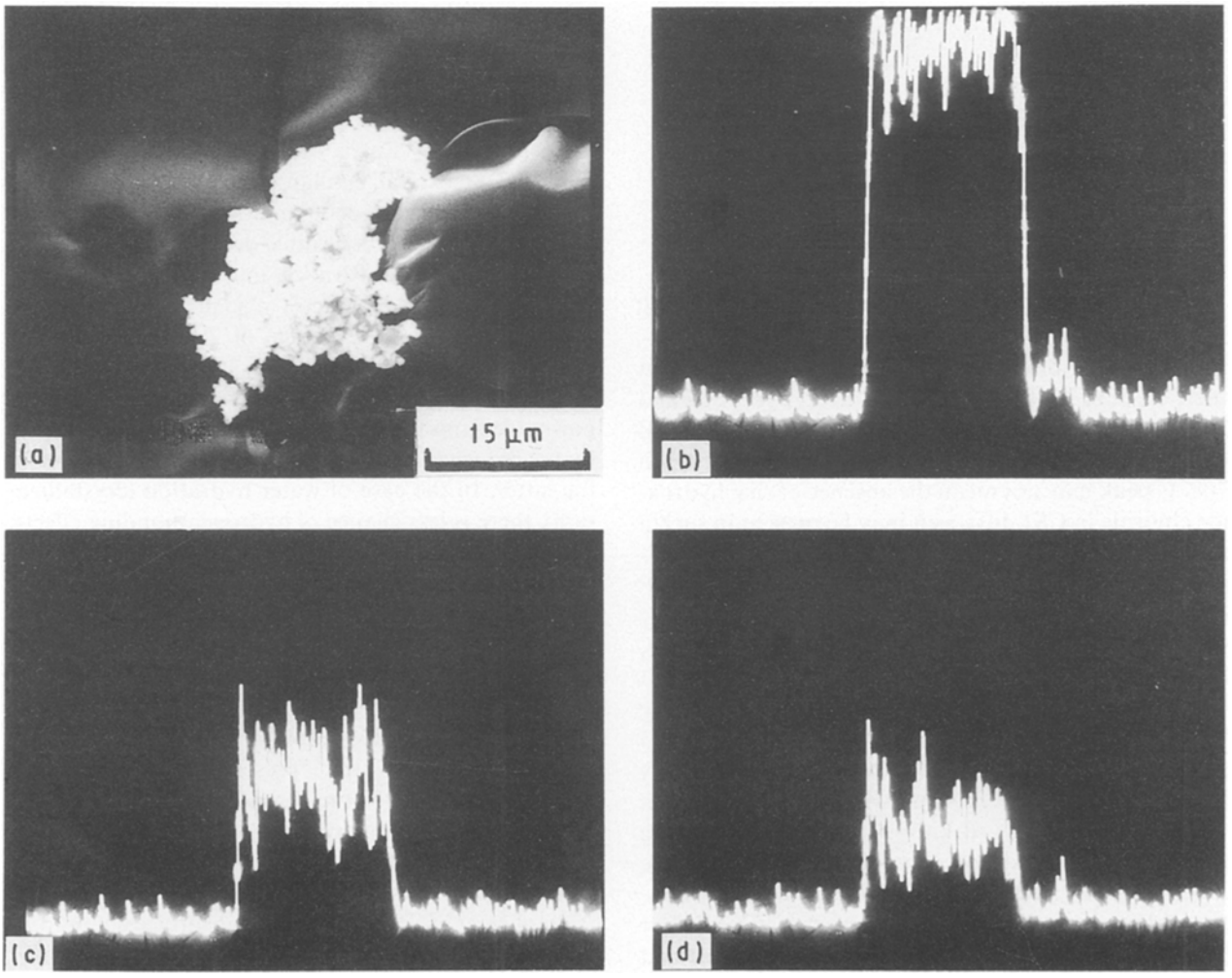

Figure 6 (a) SEM micrograph and line-scanning analyses of CS1 dust: (b) FeK_α, (c) ZnK_α, (d) MnK_α.

$Zn(OH)_2$, $CaSiO_3$ and $ZnCl_2$. These results support the conclusion that $ZnCl_2 \cdot 4Zn(OH)_2 \cdot H_2O$ exists as an extremely thin coating on the EAF-dust-particle surface.

3.2. Acid leaching

CS1 dust was leached with different concentrations of acid (using a solid/liquid mass ratio of 1/10 and a leaching time of 2 h), since the rate of ferrite dissolu-

tion in H_2SO_4 or HCl is five orders of magnitude lower than that of zinc oxide [17]. The leached residues were then examined by XRD and the results are presented in Fig. 12. After 1 h of 0.5 N HCl, ZnO and $ZnCl_2 \cdot 4Zn(OH)_2 \cdot H_2O$ peaks disappeared completely, while those of spinel ferrite became prominent. The leached residues were also analysed by i.r., and the results are presented in Fig. 13. When HCl concentrations exceed 1 h in 0.5 N, the absorption band of $ZnCl_2 \cdot 4Zn(OH)_2 \cdot H_2O$ disappears leaving only those of spinel ferrite. The residue of CS1 dust (leached with 0.5 N HCl) was investigated by AES, and the results are presented in Fig. 14. Note the presence of elements Si, C, Ca, O, Mn, Fe and Zn. In order to determine whether ZnO and $ZnCl_2 \cdot 4Zn(OH)_2 \cdot H_2O$ dissolved completely at a HCl concentration greater than 0.5 N, XRD, i.r., AES and SIMS analyses were carried out. SEM micrographs of the leached residues are given in Fig. 15, confirming that ZnO and $ZnCl_2 \cdot 4Zn(OH)_2 \cdot H_2O$ were leached out.

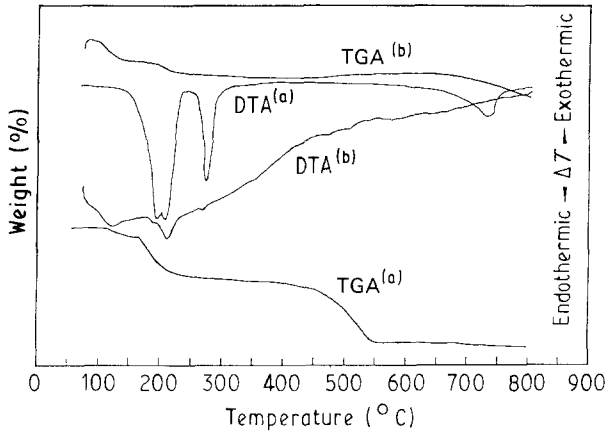

Figure 7 DTA and TGA curves of: (a) $ZnCl_2 \cdot 4Zn(OH)_2$ and $ZnCl_2 \cdot 4Zn(OH)_2 \cdot H_2O$ (after Srivastava and Secco, 1967 [12]), (b) CS1 dust.

3.3. Generation of $ZnCl_2 \cdot 4Zn(OH)_2 \cdot H_2O$

For raw material, a number of EAF steelmaking factories use scrap iron and steel which is usually coated with zinc metal as a protection against corrosion. Wire galvanizing is one such protection process that utilizes zinc coating. Following annealing, wire (iron or steel) is passed through a bath of hot HCl to remove surface iron oxide. Next, the cleaned and thoroughly washed wire is passed through a hot solution of zinc chloride or zinc ammonium chloride flux to protect the surface from oxidation during drying, and then straight into molten zinc which forms a protective coating about the wire [18]. When galvanized iron or steel wire becomes scrap and is melted in an EAF, both zinc metal and zinc chloride are easily vapourized due to their relatively low boiling points of

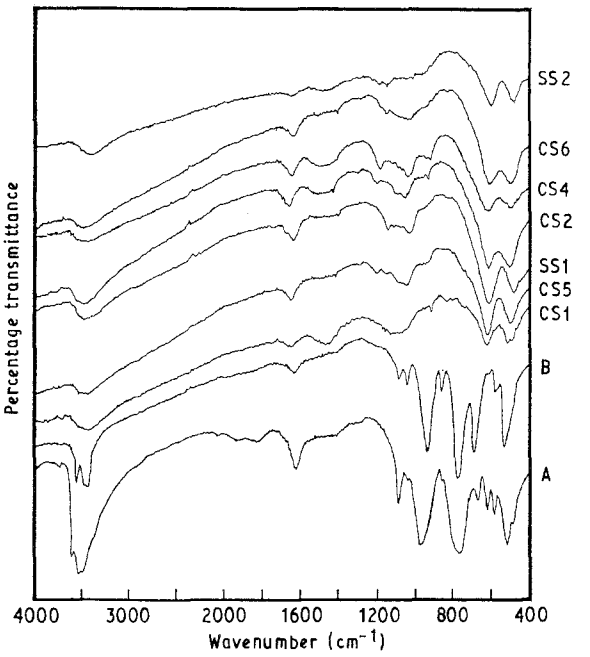

Figure 9 I.r. spectra of EAF dust: A, $ZnCl_2 \cdot 4Zn(OH)_2 \cdot H_2O$; B, $ZnCl_2 \cdot 4Zn(OH)_2$.

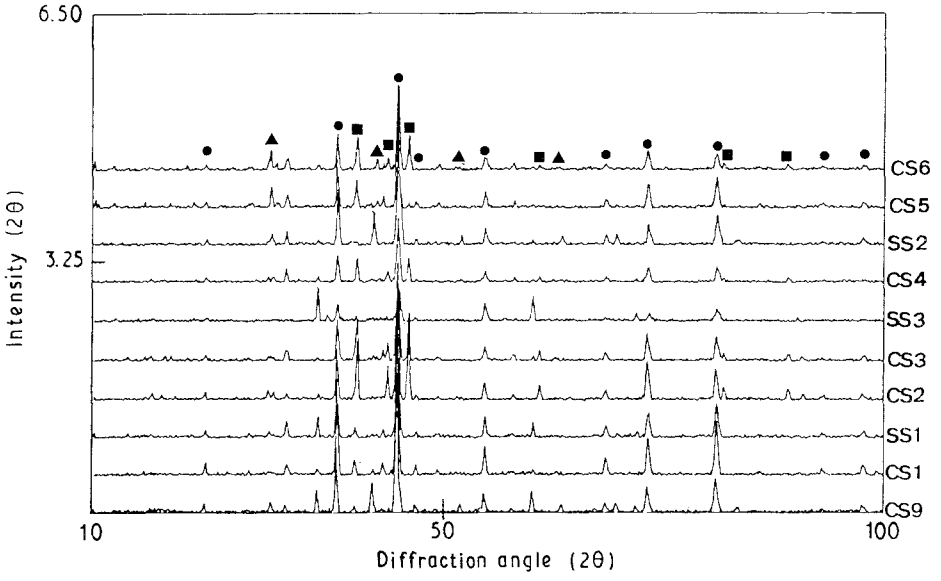

Figure 8 XRD patterns of EAF dust after being calcined for 4 h at 600 °C: ● spinel ferrite, ■ ZnO, ▲ α- Fe_2O_3.

907 and 732 °C [19], respectively. Note that zinc vapour will be oxidized completely when in contact with oxygen. Moreover, scrap iron and steel are usually found mixed with organic compounds (i.e. paints, plastics and solvents) made up of chloride compounds, such as polyvinyl chloride (PVC) and methylchloroform. In fact, HCl was found to be present in PVC materials that decomposed above 375 °C [20]. When HCl gas comes in contact with ZnO, the following reaction will take place:

$$ZnO + 2HCl \rightarrow ZnCl_2 + H_2O \cdots \quad (3)$$

Consequently, ZnO and $ZnCl_2$ simultaneously exist in both the generation process of EAF dust and after condensation occurs.

In order to determine whether the generation of $ZnCl_2 \cdot 4Zn(OH)_2 \cdot H_2O$ was possible, the bottom of a desiccator was filled with water and a mixture containing a 1:4 molar ratio of ZnO to $ZnCl_2$ was placed on the platform above this. The vessel was then sealed and left to stand at room temperature for 12 h. The

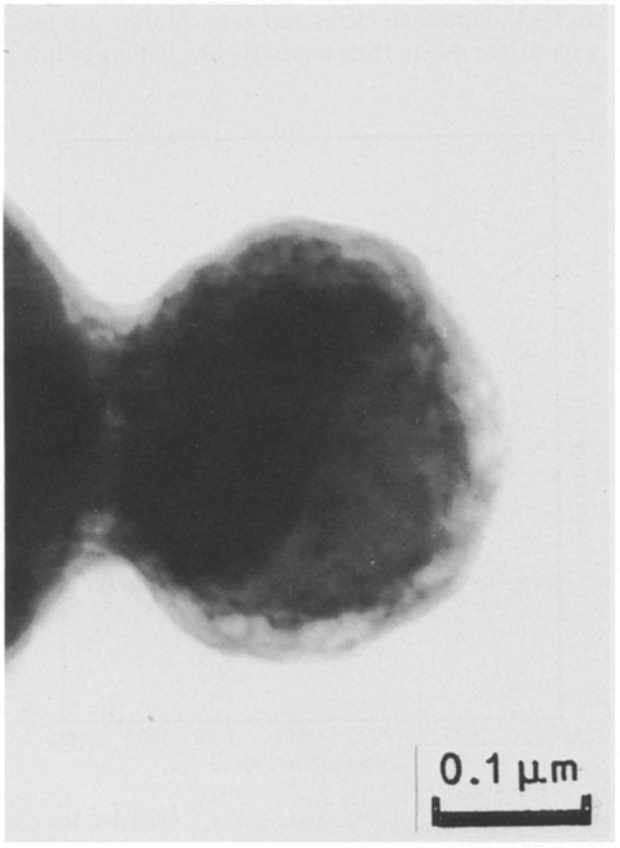

Figure 10 TEM micrograph of CS1 dust.

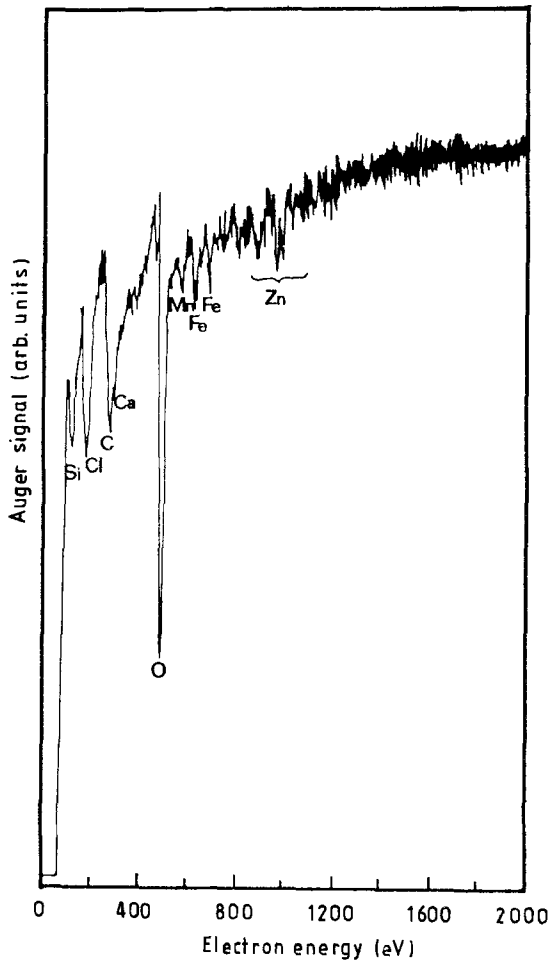

Figure 11 Auger spectrum of the particle surface of CS1 dust.

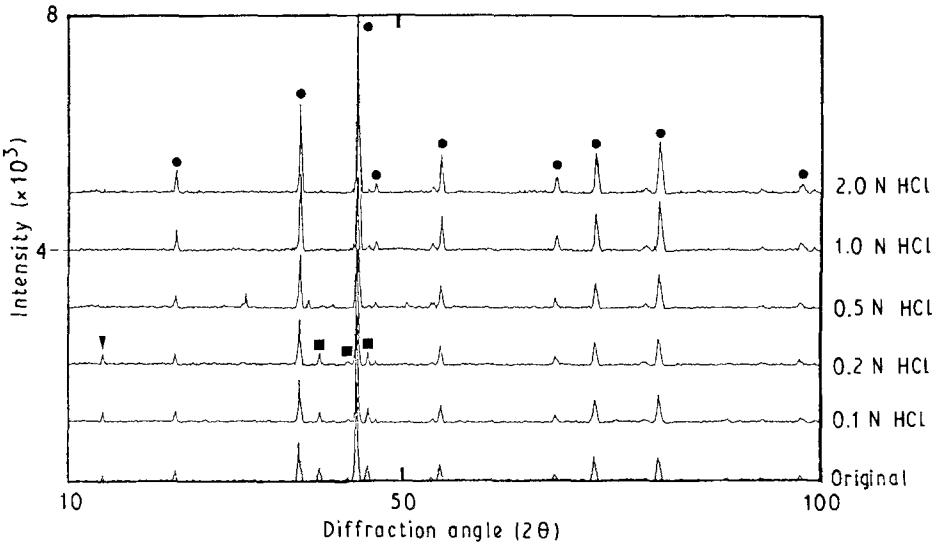

Figure 12 XRD patterns of CS1 dust leached by 0.1, 0.2, 0.5, 1.0 and 2.0 N HCl: (●) spinel ferrite, (■) ZnO, (▼) $ZnCl_2 \cdot 4Zn(OH)_2 \cdot H_2O$.

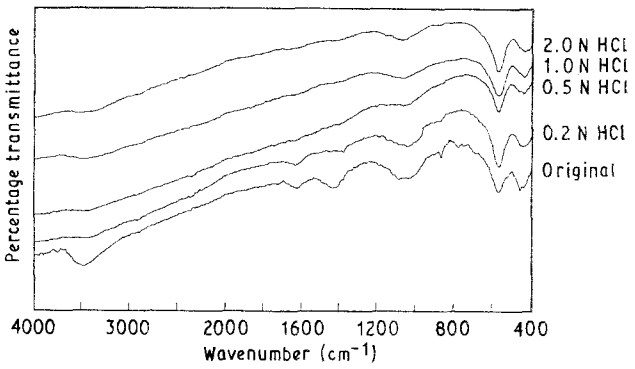

Figure 13 I.r. spectra of CS1 dust leached by 0.2, 0.5, 1.0 and 2.0 N HCl.

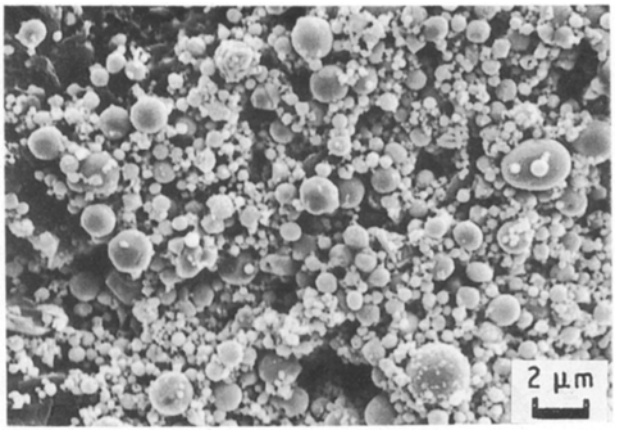

Figure 15 SEM micrograph of CS1 dust leached with 0.5 N HCl.

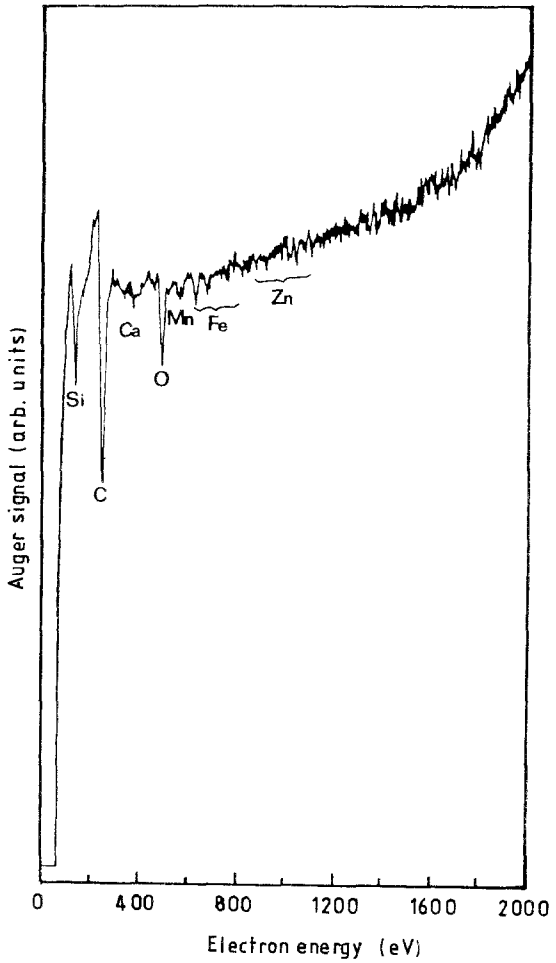

Figure 14 Auger spectrum of the particle surface of CS1 dust leached with 0.5 N HCl.

reaction product (as determined by a comparison with Srivastava and Secco's DTA/TGA and i.r. results) was indeed $ZnCl_2 \cdot 4Zn(OH)_2 \cdot H_2O$. It is interesting to note that our XRD pattern for $ZnCl_2 \cdot 4Zn(OH)_2$ is superimposable on that obtained for $ZnCl_2 \cdot 4Zn(OH)_2 \cdot H_2O$ in JCPDS (joint committee on powder diffraction standards).

DTA/TGA results indicate that $ZnCl_2 \cdot 4Zn(OH)_2 \cdot H_2O$ decomposes at 187–200 °C, therefore, it is a thermally unstable material in the EAF process system, where all the parts (except those of the gas cooler and bag house) are heated to over 200 °C, and hence it will not be generated before the EAF dust passes through the gas cooler. Due to $ZnCl_2$'s deliquescent nature [19], it binds together the small particles of Mn–Zn ferrite in EAF dust and, at the same time, reacts with the ZnO adhering to the Mn–Zn ferrite particles to form the compound $ZnCl_2 \cdot 4Zn(OH)_2 \cdot H_2O$.

4. Conclusions

1. An examination of the XRD patterns of EAF dust revealed that the major crystal phases are spinel ferrite and ZnO, and that the compound $ZnCl_2 \cdot 4Zn(OH)_2$ may also exist, as evidenced by several weaker peaks. DTA/TGA and i.r. data confirmed that the weaker peaks were due to $ZnCl_2 \cdot 4Zn(OH)_2 \cdot H_2O$.

2. EPMA analyses of EAF dust indicated that the small agglomerated spherical particles were composed of various components of Mn–Zn ferrite.

3. AES and SIMS analyses revealed that $ZnCl_2 \cdot 4Zn(OH)_2 \cdot H_2O$ exists as an extremely thin coating on the Mn–Zn ferrite particles.

4. EAF dusts are a combination of small spherical Mn–Zn ferrite particles and ZnO which are agglomerated with $ZnCl_2 \cdot 4Zn(OH)_2 \cdot H_2O$.

5. Treatment of EAF dust with 1N HCl solution dissolves ZnO and $ZnCl_2 \cdot 4Zn(OH)_2 \cdot H_2O$, the binding substance, leaving loosely aggregated Mn–Zn ferrite material.

6. $ZnCl_2$ is condensed after dust passes through the EAF gas cooler where it reacts with the ZnO adhering to Mn–Zn ferrite particles, forming the compound $ZnCl_2 \cdot 4Zn(OH)_2 \cdot H_2O$.

References

1. L. L. STEPHEN, F. L. WAYNE, G. S. JANET and W. K. GARY, Bureau of B Mines, Report of Investigation 8750 (1983).
2. R. KALTENHAUSER, in "Disposal, recycling and recovery of electric furnace exhaust dust" edited by Iron & Steel Society AIME (AIME, 1987) 31.
3. W. M. DRESSEL, P. G. BARNARD and M. M. FINE, US Bureau of Mines. Report of Investigation 7927 (1974).
4. E. G. VALDEZ and K. C. DEAN, US Bureau of Mines. Report of Investigation 8000 (1975).
5. E. R. KRISHNAN and W. F. KEMNER, in "Disposal, recycling and recovery of electric furnace exhaust dust", edited by Iron and Steel Society, AIME (AIME, 1987) p. 77.

6. J. G. EACOTT, M. C. ROBINSON, E. BUSSE, J. E. BURGENER and P. E. BURGENER, *CIM Bull.* (1984) 75.
7. J. FRENAY, J. HISSEL and S. FERIAY, in "Recycling and secondary recovery of metals", edited by P. R. Taylor, H. Y. Sohn and N. Jarrett (The Metallurgical Society Inc., 1985) p. 195.
8. E. R. KRISHNAN, in Environ. Prog. (1983) 184.
9. B. K. THOMAS and D. J. FRAY, *Metall. Trans. B* **12** (1981) 281.
10. M. C. JHA and P. C. DUYVESTEYN, in "Recycling and secondary recovery of metals", edited by P. R. Taylor, H. Y. Sohn and N. Jarrett (The Metallurgical Society Inc., 1985) p. 143.
11. D. J. FRAY, *Trans. Inst. Min. Metall.* **95** (1986) 55.
12. O. K. SRIVASTAVA and E. A. SECCO, *Can. J. Chem.* **45** (1967) 579.
13. J. A. GADSDEN, in "Infrared spectra of minerals and related inorganic compounds" (Butterworths, 1975) pp. 14–16, 48, 117.
14. U. ENZ, in "Magnetism and magnetic materials: Historical developments," Vol. 3, edited by E. P. Wonlfarth (1982) p. 285.
15. YUTAKA TAMAURA, PERLAS V. BUDUAN and TAKASHI KATSURA, *J. Chem. Soc. Dalton Trans.* (1981) 1807.
16. O. K. SRIVASTAVA and E. A. SECCO, *Can. J. Chem.* **45** (1967) 585.
17. W. RIESENKAMPF, M. HAMAKIEWICZ, S. BALOGOPALAN, S. JASIENSKA, J. KORECKI and Z. OBUSZKO, *Trans. Inst. Min. Metal.* **93** (1984) 59.
18. H. E. MCGANNON, in "The making, shaping and treating of steel", 9th Edition (United States Steel, 1970) p. 856.
19. M. WINDHOLZ, S. BUDAVARI, F. B. ROSEMARY and S. O. ELIZABETH in "The Merck Index – An encyclopedia of chemicals, drugs and biologicals", 10th Edition (1983) pp. 1456, 7.
20. J. LEIDNER, in "Plastics waste–recovery of economic value" (Marcel Dekker, New York and Basel, 1981) p. 293.

Received 2 January
and accepted 24 August 1992